Monthly Notices
of the
ROYAL ASTRONOMICAL SOCIETY

MNRAS **497,** 809–817 (2020)
Advance Access publication 2020 July 07

doi:10.1093/mnras/staa1971

# NGTS clusters survey – II. White-light flares from the youngest stars in Orion

James A. G. Jackman [1,2]★ Peter J. Wheatley [1,2] Jack S. Acton,[3] David R. Anderson [1,2] Claudia Belardi,[3] Matthew R. Burleigh,[3] Sarah L. Casewell,[3] Philipp Eigmüller,[4] Samuel Gill,[1,2] Edward Gillen [5]† Michael R. Goad,[3] Andrew Grange,[3] Simon T. Hodgkin,[6] James S. Jenkins [7,8] James McCormac,[1,2] Maximiliano Moyano,[9] Didier Queloz,[5] Liam Raynard,[3] Rosanna H. Tilbrook,[3] Christopher A. Watson[10] and Richard G. West [1,2]

[1]*Department of Physics, University of Warwick, Gibbet Hill Road, Coventry CV4 7AL, UK*
[2]*Centre for Exoplanets and Habitability, University of Warwick, Gibbet Hill Road, Coventry CV4 7AL, UK*
[3]*School of Physics and Astronomy, University of Leicester, Leicester LE1 7RH, UK*
[4]*Institute of Planetary Research, German Aerospace Center, Rutherfordstrasse 2, D-12489 Berlin, Germany*
[5]*Astrophysics Group, Cavendish Laboratory, J.J. Thomson Avenue, Cambridge CB3 0HE, UK*
[6]*Institute of Astronomy, University of Cambridge, Madingley Rise, Cambridge CB3 0HA, UK*
[7]*Departamento de Astronomía, Universidad de Chile, Camino El Observatorio 1515, Las Condes, Casilla 36-D, Santiago, Chile*
[8]*Centro de Astrofísica y Tecnologías Afines (CATA), Casilla 36-D, Santiago, Chile*
[9]*Instituto de Astronomía, Universidad Católica del Norte, Angamos 0610, Antofagasta 1270709, Chile*
[10]*Astrophysics Research Centre, School of Mathematics and Physics, Queen's University Belfast, Belfast BT7 1NN, UK*

Accepted 2020 July 2. Received 2020 June 26; in original form 2019 November 5

## ABSTRACT

We present the detection of high-energy white-light flares from pre-main-sequence stars associated with the Orion Complex, observed as part of the Next Generation Transit Survey (NGTS). With energies up to $5.2 \times 10^{35}$ erg these flares are some of the most energetic white-light flare events seen to date. We have used the NGTS observations of flaring and non-flaring stars to measure the average flare occurrence rate for 4 Myr M0–M3 stars. We have also combined our results with those from previous studies to predict average rates for flares above $1 \times 10^{35}$ erg for early M stars in nearby young associations.

**Key words:** stars: flare – stars: low-mass – stars: pre-main-sequence.

## 1 INTRODUCTION

The pre-main sequence represents the most active period in a star's lifetime, something reflected in their light curves. Material from surrounding discs passing in front the star can cause deep drops in their apparent flux (e.g. Cody et al. 2014; Ansdell et al. 2016), while accretion events can cause rapid rises in flux (e.g. Guo et al. 2018). Another source of variability is stellar flares, explosive phenomena caused by reconnection events in the stellar magnetic field (e.g. Benz & Güdel 2010). The energy released by these reconnection events accelerates charged particles that heat the stellar photosphere, resulting in intense white-light emission.

The amplitudes and measured energies from stellar flares from pre-main-sequence stars regularly dwarf those from their main-sequence counterparts (e.g. Caramazza et al. 2007; Flaccomio et al. 2018). The associated loop lengths from these flares can even dwarf the star itself, with X-ray studies measuring loop lengths of several stellar radii (e.g. Favata et al. 2005). If these loops link to a surrounding disc, these flares could drive accretion of disc material on to the star (Orlando et al. 2011; Colombo et al. 2019).

In recent years, studies of white-light flares have begun to move towards how flare properties evolve as a function of age (e.g. Chang, Byun & Hartman 2015; Davenport et al. 2019; Ilin et al. 2019). As stars age after they have reached the zero-age main sequence, they are expected to spin-down and lose angular momentum through magnetic braking. Studies of open clusters and associations of known ages have shown this occurs in a mass-dependent fashion, with higher mass stars spinning down first (e.g. Epstein & Pinsonneault 2014; Matt et al. 2015; Douglas et al. 2019). This spin-down is expected to affect the internal dynamo also, weakening it and the magnetic field it generates. This decrease in the magnetic activity with time has already been observed in extreme ultraviolet (XUV) observations that probe the coronal activity (e.g. Jackson, Davis & Wheatley 2012). A weakening of the magnetic activity is also expected to be reflected in a decrease in the measured energies and average occurrence rates of stellar flares. Indeed, recent studies have begun to see this in white-light flare observations. Davenport et al. (2019) have studied how flare occurrence rates vary with age by combining gyrochronology with the Davenport (2016) *Kepler* flare sample. They were able to derive a mass- and age-dependent model for the flare occurrence rate, however note that their results may be affected by tidal evolution of

★ E-mail: j.jackman@warwick.ac.uk
† Winton Fellow.

binaries that can bias age estimates to younger ages. By using *K2* observations of flares from stars within the 125 and 630 Myr Pleiades and Praesepe clusters, Ilin et al. (2019) measured the decrease in average flare rates between these two ages for K and M stars. They found the decrease occurs quicker than predicted from the Skumanich (1972) $t^{-1/2}$ law, suggesting they are still in a regime of time-variable spin-down that cannot be parametrised by a single law (e.g. Barnes 2010).

Measurements of average white-light flare occurrence rates so far have used clusters older than 100 Myr. Observations of systems younger than this have typically been of individual stars (e.g. Jackman et al. 2019) or been X-ray observations that probe different parts of the flare reconnection model (e.g. Stelzer et al. 2007; Flaccomio et al. 2018). During the first 100 Myr stars with masses above 0.4 $M_\odot$ form their radiative zone (Baraffe et al. 2015). Gregory, Adams & Davies (2016) found evidence that the formation of the radiative zone is accompanied by a drop in the coronal X-ray luminosity, a parameter used as a probe of stellar magnetic activity. Studies of clusters up to 100 Myr would allow us to see whether the formation of the radiative zone has an impact on the average flaring activity. Along with this we can constrain the starting point of flare occurrence rates, informing studies of flares on the habitability of the youngest exoplanetary systems.

In this work, we report the detection of white-light flares from pre-main-sequence stars in the Orion Complex with the Next Generation Transit Survey (NGTS). These stars have a weighted average age of $4.0 \pm 0.2$ Myr (Kounkel et al. 2018). We describe how the maximum energies of these flares compare with those from main-sequence stars and present measurements of the average flare occurrence rate for early M stars. We also compare our occurrence rates to those of Pleiades and Praesepe from Ilin et al. (2019) and predict upper limits on flare occurrence rates for nearby young associations.

## 2 OBSERVATIONS

NGTS is a ground-based wide-field exoplanet survey located at the Paranal Observatory in Chile. It consists of twelve 20-cm aperture telescopes with a total instantaneous field of view of 96 $deg^2$ (Wheatley et al. 2018). These telescopes obtain full frame images with a 13 s cadence. The data presented in this work were collected with NGTS between the dates of 2015 September 23 and 2016 April 20, with a total of 138 nights of observation.

In the standard mode of operations NGTS obtains light curves for all stars within its field of view brighter than $I = 16$ (Wheatley et al. 2018). We are currently searching light curves from the first year of NGTS observations (Jackman et al., in preparation) for stellar flares. To search for flares we follow the two-step method described in Jackman et al. (2018). For a given star we first search individual nights for regions where there are at least three consecutive points above 6 median absolute deviations (MADs) from the median of the night. If there are three consecutive points above 6 MADs from the median, that night is automatically flagged. Secondly, we compare the median of the night against the median of the entire light curve for that object. If the median of the night is at least 5 MADs above the median light-curve flux, then night is automatically flagged. Nights that are raised above the median of the light curve are indicative of long-duration and high-amplitude events such as the flare discussed in Jackman et al. (2019). Once this automated flagging procedure was complete, we inspected each flagged night visually and removed any false positives. Such false positives can be due to astrophysical events (e.g. short-period variable stars), man made (e.g. satellites passing through our aperture) or systematics (e.g. overlapping apertures). This method is most sensitive to the highest energy flare events.

Once we had remove any false positives from our sample, we checked the centroids of all flare candidates. Each flare is assigned to a host star, initially the star on which the aperture is placed and centred. However, if multiple stars reside within an aperture, then it is possible a flare could come from a star not in the centre of the aperture. In this case, the aperture centroid will move during the flare towards the true flaring source. By checking the centroids during each flare we can confirm each source is the correct host and reassign a host star if not.

During this flare survey we noted that one field overlapped with the southern edge of the Orion Complex. This serendipitous overlap provided an opportunity to measure the white-light flaring behaviour of some of the youngest stars on the sky.

**Table 1.** Identified groups for NGTS flare stars in Orion with ages from Kounkel et al. (2018). $N_{\rm stars,\ total}$ indicates the number of stars in our field associated with the respective group, while $N_{\rm stars,\ flare}$ is the number of those stars that flared. We use the $\rm Age_{CMD}$ in our analysis and list $\rm Age_{HR}$ for reference.

| Group | $N_{\rm stars,\ total}$ | $N_{\rm stars,\ flare}$ | $\rm Age_{CMD}$ (Myr) | $\rm Age_{HR}$ (Myr) |
|---|---|---|---|---|
| L1641N-1 | 31 | 7 | $3.47 \pm 1.89$ | $2.18 \pm 1.60$ |
| onc-1 | 4 | 2 | $3.98 \pm 1.79$ | $4.06 \pm 1.48$ |
| onc-3 | 1 | 1 | $3.31 \pm 1.72$ | $2.36 \pm 1.79$ |
| onc-8 | 1 | 1 | $3.37 \pm 1.98$ | $2.99 \pm 2.11$ |
| onc-11 | 1 | 0 | $3.58 \pm 1.34$ | $4.85 \pm 1.97$ |
| onc-15 | 1 | 0 | $2.51 \pm 1.86$ | $2.34 \pm 1.79$ |
| oriDS-1 | 19 | 5 | $3.02 \pm 1.78$ | N/A |
| oriDS-2 | 1 | 0 | $6.61 \pm 1.76$ | N/A |
| oriDS-3 | 7 | 1 | $5.13 \pm 2.14$ | N/A |
| oriDS-4 | 7 | 0 | $8.71 \pm 2.48$ | N/A |
| oriDS-5 | 2 | 1 | $5.01 \pm 1.51$ | N/A |
| oriDS-6 | 1 | 0 | $4.79 \pm 1.41$ | N/A |
| oriDS-7 | 5 | 1 | $6.01 \pm 1.65$ | N/A |
| oriDS-8 | 2 | 0 | $2.19 \pm 2.51$ | N/A |

### 2.1 Association

To identify which stars are associated with groups within Orion, we cross-matched all NGTS sources in the Orion-overlapping field with the catalogue of Kounkel et al. (2018). Using *Gaia* Data Release 2 (DR2) and Apache Point Observatory Galactic Evolution Experiment (APOGEE) data, Kounkel et al. (2018) have mapped distinct groups within the Orion Complex and their catalogue provides designations for Orion-associated stars and field stars. From this matching we identified 83 Orion-associated stars that fell within our field of view. Of these, 19 flared at least once during our observations. The smallest and largest amplitude detected flares are shown in Figs A1 and A2. The groups and ages of the stars in our sample are shown in Table 1. We can see in Table 1 that these groups have similar ages. Consequently, we have considered them as a single group of pre-main-sequence stars with an average age of $4.0 \pm 0.2$ Myr for the rest of this analysis. We calculated this age and uncertainty by taking a weighted average of the $\rm Age_{CMD}$ values presented in Table 1. The $\rm Age_{CMD}$ were calculated by Kounkel et al. (2018) using colour–magnitude diagrams used APOGEE and *Gaia* DR2 colours with PARSECmodels to obtain absolute magnitudes for all young stars in their sample, including for young stellar objects without reliable parallaxes. The $\rm Age_{HR}$ values listed in Table 1 used the

*Gaia* parallaxes and APOGEE measured effective temperatures to obtain luminosities, which were compared with PARSEC models to infer ages. The dependence on the effective temperature results in a smaller sample having $\mathrm{Age_{HR}}$ values, as seen in Table 1. Because of the lack of $\mathrm{Age_{HR}}$ values for all stars in our sample, we have used the $\mathrm{Age_{CMD}}$ in this work.

### 2.2 Stellar properties

Eight sources in our sample had effective temperatures and angular sizes measured by Kounkel et al. (2018) from APOGEE spectra. We obtained the stellar radius for these sources by combining the angular sizes with their measured distances from the Bailer-Jones et al. (2018) catalogue, using parallaxes from *Gaia* DR2 (Gaia Collaboration et al. 2016, 2018).

For the rest of our sources we performed spectral energy distribution (SED) fitting using the PHOENIX v2 spectral library (Allard, Homeier & Freytag 2012). Each source was cross-matched with the *Gaia* DR2, Two Micron All-Sky Survey (2MASS; Skrutskie et al. 2006), AAVSO Photometric All-Sky Survey (APASS; Henden & Munari 2014), Sloan Digital Sky Survey (SDSS; Aguado et al. 2019), and AllWISE (Cutri & et al. 2014) to obtain broad-band photometry. Distance information was obtained from the catalogue of Bailer-Jones et al. (2018). To account for the effects of reddening and extinction, we fit for $A_V$, with $R_V = 3.1$ (Cardelli, Clayton & Mathis 1989). $R_V$ is the ratio of the total to selective extinction. We applied a Gaussian prior on the reddening based on the values measured from APOGEE spectra for the groups in Table 1 by Kounkel et al. (2018). This was chosen overexisting dust maps of Green et al. (2019) as we found half of the stars in our sample had poor likelihoods in their dust map fits, using the criteria from Green et al. (2019).

To avoid the effects of blending between close neighbours influencing our SED fitting, we checked all sources for stars within 15 arcsec (the radius of an NGTS aperture) that might contribute significant levels of flux to the NGTS light curve. Sources that had nearby neighbours were flagged and did not have SED fits generated. Consequently, these stars (flaring and non-flaring) were not used in our analysis.

From our analysis we obtain 10 K and 49 M stars in our sample. The rest of the sample either had effective temperatures hotter than K spectral type, or did not have a reliable SED fit.

### 2.3 Flare properties

To calculate flare energies we follow an adjusted version of the method from Shibayama et al. (2013). The original method uses the observed flare amplitude to normalise an assumed $9000 \pm 500$ K flare blackbody (e.g. Hawley & Fisher 1992) relative to the quiescent stellar spectrum within the observed bandpass. The bolometric flare energy is measured by integrating over the renormalised 9000 K flare spectrum at each observed time. We have modified this method in our analysis to account for the effects of reddening on the observed flare and stellar spectrum (e.g. Paudel et al. 2018b), using the fitted values of $A_V$ from Section 2.2. We used the average Milky Way extinction model from Cardelli et al. (1989) in this method.

When applying this method we assumed the underlying quiescent stellar flux could be modelled with a linear baseline between the start and end of the flare. For the stellar properties (to generate the quiescent stellar spectrum) we use the radii and effective temperatures from Section 2.2.

We calculated the $t_{1/2}$ duration and amplitude for all flares. These values are listed in Table 2. The $t_{1/2}$ duration is a commonly used measure of flare duration (e.g. Davenport et al. 2014) and is defined as the time spent above half of the flare amplitude. We calculated the amplitude following the method from Hawley et al. (2014) using $\frac{\Delta F}{F} = \frac{F - F_\mathrm{o}}{F_\mathrm{o}}$, where $F_\mathrm{o}$ is the out-of-flare flux. The value of $F_\mathrm{o}$ is calculated from the median of the flux preceding the start of the flare. As these parameters are independent of spectral type we have listed both $t_{1/2}$ and the amplitude for all flares in Table 2.

## 3 RESULTS AND DISCUSSION

From an analysis of 83 stars associated with the Orion Complex that were observed with NGTS, we detected 26 flares from 17 stars. 16 of these 17 flare stars had effective temperatures from our SED fits or the Kounkel et al. (2018) sample, which corresponded to spectral types between G3 and M3. 12 stars were M spectral type and four were K. The observed flares had energies ranging between $6.7 \times 10^{33}$ and $5.2 \times 10^{35}$ erg.

The presence of a flare from a G3 star in our sample is interesting due to the rarer nature of flares from these stars. However, investigating this source further shows it has previously been classified as K4 from low-resolution spectra by Pravdo & Angelini (1995) and as G8 from spectroscopic observations by Strom et al. (1990). Based on these observations it is likely this source is later in spectral type than our SED fitting suggests, however without an exact classification we have chosen to leave it out from our energy analysis. However, we still list the NGTS flare amplitude and duration for this star in Table 2, as these do not depend on the stellar properties.

### 3.1 Maximum flare energy

In Fig. 1, we have compared the maximum flare energy of the Orion-associated stars to main-sequence stars observed with *Kepler* from Yang & Liu (2019). The Orion-associated stars reside at the top of the energy envelope with maximum flare energies between $2.5 \times 10^{34}$ and $5.2 \times 10^{35}$ erg. These energies are similar to those observed by Flaccomio et al. (2018) from simultaneous mid-infrared, optical, and X-ray observations of pre-main-sequence stars in the ∼3-Myr old NGC 2264 star-forming region. Adopting the ratio between optical and X-ray energies (0.5–8.0 keV) from Flaccomio et al. (2018), we estimate that our maximum X-ray flare energies are between $1.4 \times 10^{33}$ and $7.7 \times 10^{34}$ erg.

Our measured bolometric flare energies, while similar to the Flaccomio et al. (2018) sample, reside towards the lower end of their measured energies. This is possibly due the Flaccomio et al. (2018) sample observing more stars in their study, approximately 500 stars for 60 d with the *Convection, Rotation and planetary Transits* (*CoRoT*). Consequently, this suggests that while our flares have high energies, they are not at the maximum limit of flare energies for these young stars. Further observations are therefore required to reach the maximum flare energy limit for 4 Myr old stars.

We have also measured the bolometric equivalent durations (EDs) for each flare in our sample, using the bolometric flare energies and our SED fits from Section 2.2. The ED is the amount of time required for the quiescent luminosity of the star to emit an energy equal to an observed flare (e.g. Hawley et al. 2014). It is usually expressed in units of time. We calculated our EDs by dividing the bolometric flare energies by the stellar bolometric luminosity. We calculated the bolometric luminosity by integrating in wavelength over our best-fitting SED fits (after removing the effect of extinction) and multiplying by $4\pi d^2$, where $d$ is the distance. Fig. 2 shows the maximum bolometric ED for each star in our sample, showing that the equivalent durations have values up to 15 min, however the

**Table 2.** Detected flares and their measured properties. The SpT source column indicates the method used to obtain the spectral type for this source. 2MASS J05362219−0716064 was marked in our analysis as a blended source, so does not have a measured flare energy and its amplitude is marked as a lower limit ([ll]). The spectral type of 2MASS J05354229−0701538 is marked with an asterisk (∗) for reasons discussed in Section 3. K18 indicates the spectral type is taken from Kounkel et al. (2018).

| 2MASS source ID | *Gaia* DR2 source ID | SpT | SpT source | Energy (erg) | Amplitude | $t_{1/2}$ duration (min) |
|---|---|---|---|---|---|---|
| 2MASS J05354229−0701538 | 3016493834224711552 | G3∗ | SED | | 0.16 | 49.50 |
| 2MASS J05331830−0701552 | 3016526991372177664 | K6.5 | SED | $2.77^{+0.85}_{-0.65} \times 10^{35}$ | 0.52 | 26.13 |
| 2MASS J05331830−0701552 | 3016526991372177664 | K6.5 | SED | $1.87^{+0.58}_{-0.44} \times 10^{35}$ | 0.35 | 8.28 |
| 2MASS J05265619−0706548 | 3016662403101758720 | M0.5 | SED | $9.64^{+3.44}_{-2.53} \times 10^{34}$ | 0.59 | 15.35 |
| 2MASS J05265619−0706548 | 3016662403101758720 | M0.5 | SED | $1.01^{+0.32}_{-0.24} \times 10^{35}$ | 0.84 | 10.87 |
| 2MASS J05312392−0709304 | 3016615055382512768 | M0 | SED | $4.24^{+0.94}_{-0.77} \times 10^{34}$ | 0.61 | 4.62 |
| 2MASS J05313541−0710550 | 3016614402547478784 | M1.5 | SED | $1.76^{+0.38}_{-0.31} \times 10^{35}$ | 0.46 | 21.63 |
| 2MASS J05314319−0717409 | 3016424736790884736 | M1.5 | SED | $1.40^{+1.33}_{-0.68} \times 10^{35}$ | 1.23 | 61.00 |
| 2MASS J05340216−0717390 | 3016505963212457088 | M3 | SED | $2.70^{+1.02}_{-0.74} \times 10^{34}$ | 0.71 | 1.70 |
| 2MASS J05340216−0717390 | 3016505963212457088 | M3 | SED | $6.98^{+2.51}_{-1.85} \times 10^{34}$ | 0.80 | 23.65 |
| 2MASS J05340216−0717390 | 3016505963212457088 | M3 | SED | $3.68^{+1.40}_{-1.01} \times 10^{35}$ | 1.10 | 48.87 |
| 2MASS J05362219−0716064 | 3016469060853517824 | M1.5 | K18 | | $0.44^{ll}$ | 23.95 |
| 2MASS J05350988−0718045 | 3016457000585375872 | M2 | SED | $1.70^{+0.40}_{-0.32} \times 10^{35}$ | 1.03 | 8.55 |
| 2MASS J05351113−0719063 | 3016456210311395456 | M1 | SED | $9.08^{+2.66}_{-2.06} \times 10^{34}$ | 1.16 | 4.42 |
| 2MASS J05304799−0731323 | 3016413501156518400 | K6 | SED | $4.66^{+4.93}_{-2.40} \times 10^{35}$ | 0.30 | 21.80 |
| 2MASS J05304799−0731323 | 3016413501156518400 | K6 | SED | $2.12^{+1.86}_{-0.99} \times 10^{35}$ | 0.14 | 25.32 |
| 2MASS J05295834−0738069 | 3016388315468339200 | K7 | SED | $3.29^{+0.76}_{-0.62} \times 10^{34}$ | 0.27 | 2.52 |
| 2MASS J05295834−0738069 | 3016388315468339200 | K7 | SED | $2.64^{+0.60}_{-0.49} \times 10^{35}$ | 0.89 | 60.55 |
| 2MASS J05273635−0744059 | 3015081163645266304 | M1.5 | SED | $5.64^{+1.64}_{-1.27} \times 10^{34}$ | 0.38 | 8.60 |
| 2MASS J05295183−0750306 | 3016374743371710592 | K5.5 | SED | $5.22^{+1.28}_{-1.03} \times 10^{35}$ | 0.41 | 24.97 |
| 2MASS J05295183−0750306 | 3016374743371710592 | K5.5 | SED | $3.51^{+0.83}_{-0.67} \times 10^{35}$ | 0.25 | 19.45 |
| 2MASS J05295183−0750306 | 3016374743371710592 | K5.5 | SED | $9.93^{+2.64}_{-2.09} \times 10^{34}$ | 0.30 | 12.35 |
| 2MASS J05350942−0749194 | 3015674698061271936 | M3 | SED | $3.09^{+0.88}_{-0.68} \times 10^{35}$ | 3.47 | 7.68 |
| 2MASS J05293055−0754194 | 3014873669481488896 | M1.5 | SED | $2.54^{+0.42}_{-0.36} \times 10^{34}$ | 0.40 | 8.22 |
| 2MASS J05340890−0912415 | 3013742546894832384 | M0.5 | SED | $6.66^{+1.91}_{-1.49} \times 10^{33}$ | 0.56 | 1.28 |
| 2MASS J05340890−0912415 | 3013742546894832384 | M0.5 | SED | $1.08^{+0.31}_{-0.24} \times 10^{35}$ | 0.46 | 22.40 |

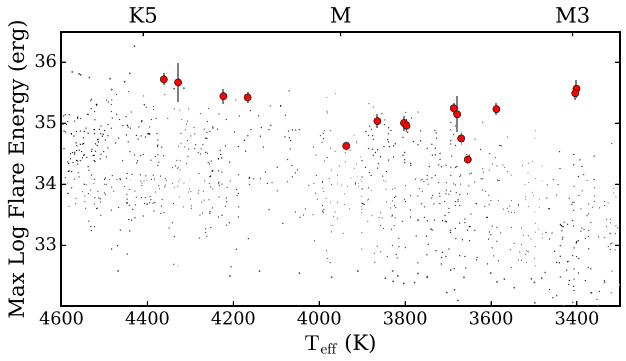


**Figure 1.** Maximum observed bolometric flare energy against effective temperature for our detected flaring stars. The red circles are the stars observed with NGTS. The underlying black points represent stars from Yang & Liu (2019), using a posteriori corrected long cadence *Kepler* observations. Note how the young Orion-associated sources detected in our survey appear to flare with the highest observed energies. We note the possibility of some stars with lower maximum flare energies in our sample that may have been missed by the detection method discussed in Section 2.

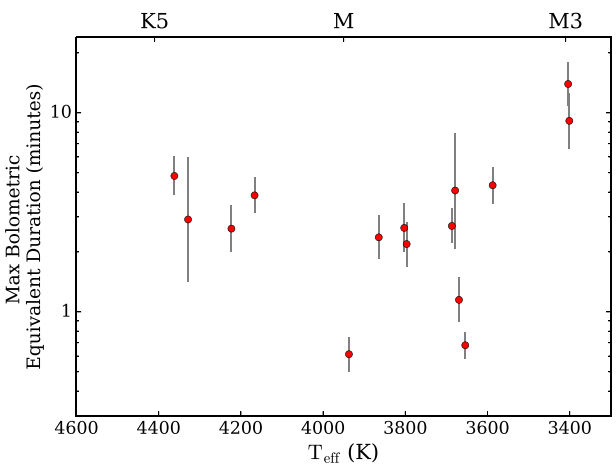


**Figure 2.** Maximum observed equivalent duration (in min) against effective temperature for our detected flaring stars. We have calculated this using our measured bolometric energies and dereddened SEDs from Section 2.2.

majority seem to have values of a few minutes. These values are lower than those reported for rare extreme flare events from other pre-main-sequence stars (e.g. Paudel et al. 2018a; Jackman et al. 2019) that can stretch to hours (although the ED is often reported for a single filter, which can change measured values; e.g. Hawley et al. 2014). This again suggests that our sample, while exhibiting high flare energies, has not reached the maximum flare energy limit for these young stars, something which will be probed in future studies.

### 3.2 Flare occurrence rate of M stars

Previous studies (e.g. Lacy, Moffett & Evans 1976; Hilton et al. 2011; Hawley et al. 2014) have shown that flares occur with a power-law

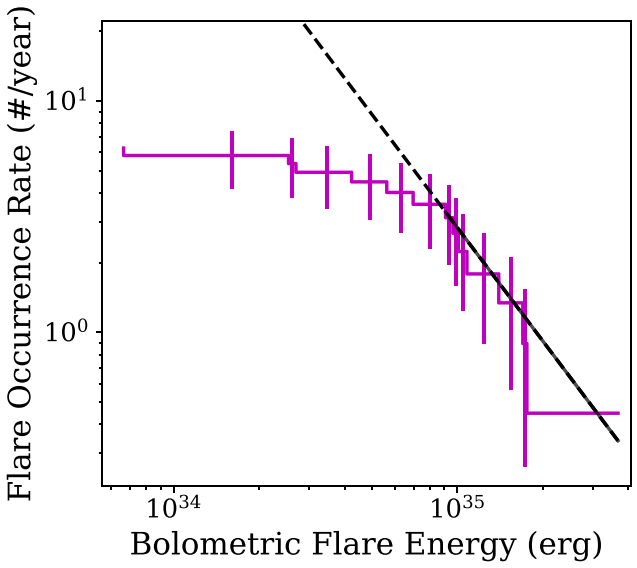


**Figure 3.** Flare occurrence rate with energy for 4.0 ± 0.2 Myr M stars associated with Orion. These stars were selected to have effective temperatures between 3400 and 3940 K, approximately equivalent to M0–M3. The black solid line indicates the best-fitting power law in our fitting range, while the dashed line is this fit extrapolated over our measured energy range. The best-fitting parameters are $\alpha = 2.63 \pm 0.62$ ($\beta = -1.63 \pm 0.62$) and $C = 57.4 \pm 21.9$.

distribution in energy. This is typically written as

$$\mathrm{d}N(E) \propto E^{-\alpha}\mathrm{d}E, \quad (1)$$

where $E$ is the flare energy and $\alpha$ is the power-law index. From this, a linear relation for the cumulative flare frequency distribution (CFFD) can be written as

$$\log \nu = C + \beta \log E, \quad (2)$$

where $\nu$ is the cumulative flare frequency, $C$ is a normalization constant, and $\beta = 1 - \alpha$ (Hawley et al. 2014). The value of $\alpha$ dictates how often high-energy flares occur relative to those of lower energy and has been observed to vary across different spectral types. For example, the Sun has $\alpha \approx 1.75$ (e.g. Crosby, Aschwanden & Dennis 1993; Shimizu 1995; Aschwanden et al. 2000), while ultracool dwarfs have had measured $\alpha$ values from 1.4 to 2 (e.g. Paudel et al. 2018a).

In Fig. 3, we have plotted the average flare occurrence rate for stars in our Orion-associated sample. This was done for stars with effective temperatures between 3400 and 3940 K, representative of early M (M0–M3) in spectral type (e.g. Pecaut & Mamajek 2013). To fit the power law shown in Fig. 3 we have used the PYTHON POWERLAW package (Alstott, Bullmore & Plenz 2014). POWERLAW is designed for fitting to heavy-tailed distributions and has been used previously for analysis of flare occurrence rates (e.g. Lin et al. 2019).

To make sure our sample is complete in terms of the detected flare energies, we performed flare injection and retrieval tests, following a similar methodology to those employed by Davenport (2016) and Ilin et al. (2019). We first injected 1000 artificial flares into the light curves of every M star in our sample. These flares were generated using the Davenport et al. (2014) empirical flare model. The amplitude of each flare was chosen randomly to have a value from between 0.01 and 3.5 times the median of an object's light curve. The $t_{1/2}$ time-scale for each flare was chosen randomly from between 30 s and 70 min, to encompass the full range of detected flares. The automated detection method outlined in Section 2 was then run for each object on every night with an injected flare. We calculated the energies of each injected flare on a star-by-star basis, applying the energy calculation from Section 2.3 to the artificially generated flare. Injected flares were given a flag of 1 if they were automatically detected by our method, 0 if not.

The fraction of recovered flares were calculated as a function of energy for each star, using 20 bins in energy. Following Davenport (2016), the recovery fraction was smoothed using a Wiener filter of three bins, to smooth any jumps and drops between bins. For each star we measured the flare energy at which at least 68 per cent of flares were retrieved, which was recorded for each star, as in Davenport (2016).

To ensure a complete sample when calculating the flare occurrence rate and when fitting the associated power law, an energy limit was used. For a given energy limit, only stars with a 68 per cent recovery fraction energy below this limit were used in calculating the average flare occurrence rate. This applied whether or not a star had any detected flares within its NGTS light curve. The power law itself, as seen in Fig. 3, was fit only to flares (from stars within this complete sample) with energies above the chosen energy limit. To select an energy limit, we tested a series of values to maximize the number of flares used in our power-law fitting, without compromising the total number of stars used. Low energy limit values would exclude most stars (and their flares) from use in the flare occurrence rate fitting. Very high energy limit values, while including all stars in the sample, would have very few flares to fit the power law to. We found a value of $9 \times 10^{34}$ erg best satisfied this compromise and was thus used as our energy limit.

29 stars in our 3400–3940 K sample (40 stars in total) had 68 per cent recovery fraction energies below our limit of $9 \times 10^{34}$ erg, and were used in our occurrence rate analysis. 10 of these stars had a detected flare. Eight flares (from seven stars) had energies above the $9 \times 10^{34}$ erg, to which we fitted a power-law distribution. Six flares (from five stars) had energies below this threshold and were not used in our power-law fitting. Some stars in our sample flared more than once, with energies above and below $9 \times 10^{34}$ erg. The full sample of flares detected from stars in the 3400–3940 K sample, along with the 68 per cent completeness energy for each star, is presented in Table B1. The full sample of completeness energies for each individual star, flaring and non-flaring, in the 3400–3940 K sample is presented in Table B2.

From fitting our sample above this threshold we measured $\alpha = 2.63 \pm 0.62$ ($\beta = -1.63 \pm 0.62$) and $C = 57.4 \pm 21.9$. An $\alpha$ value greater than 2 indicates that lower energy flares dominate the total flare energy distribution. $\alpha > 2$ has also been noted in previous works as a requirement for low-energy flares to heat solar and stellar coronas (e.g. Doyle & Butler 1985; Parker 1988; Güdel et al. 2003). With our sample we are not able to confidently rule out high-energy flares dominating the distribution, although we note the possibility that flares may be a significant contributor to the quiescent magnetic environment of young M stars. This value is also consistent with the value of $\alpha = 2.2 \pm 0.2$ measured by Caramazza et al. (2007) for X-ray flares from Orion-associated 0.1–0.3 $M_\odot$ stars.

From our power-law fit in Fig. 3 we estimate that the average 3400–3940 K star in the Orion Complex flares with an energy above $10^{35}$ erg once every 130 d. This is almost 1000 times the rate measured by Lin et al. (2019) for M dwarfs using *K2* observations, highlighting how active these pre-main-sequence sources are.

**Table 3.** Predictions of the average flare occurrence rate for some nearby young associations, for flare energies above $1 \times 10^{35}$ erg. We have calculated these by combining our measured occurrence rates with those extrapolated from Ilin et al. (2019). For intermediate-age clusters we linearly interpolated between measured samples. The ∗ indicates these are our measured values for Orion. The ‡ indicates these are the Ilin et al. (2019) extrapolated values for Pleiades and Praesepe, again shown for reference. Also shown is the number of flares in each sample. 'c' indicates a predicted value that has been calculated from the Orion, Pleiades, and Praesepe samples. 'e' indicates an estimate uses the extrapolated Ilin et al. (2019) occurrence rates. Quoted ages for groups other than Orion, Pleiades, and Praesepe come from Bell, Mamajek & Naylor (2015).

| Cluster | Age (Myr) | 3500–3750 K (# $yr^{-1}$) | $n_{flares}$ | 3750–4000 K (# $yr^{-1}$) | $n_{flares}$ |
|---|---|---|---|---|---|
| Orion∗ | 4 | 2.0 | 5 | 2.3 | 6 |
| Beta Pictoris | 24 | 1.7 | c | 2.0 | c |
| Carina | 45 | 1.3 | c | 1.6 | c |
| Pleiades‡ | 125 | $7.3 \times 10^{-2}$ | e | $2.5 \times 10^{-1}$ | e |
| AB Doradus | 149 | $7.3 \times 10^{-2}$ | e | $2.4 \times 10^{-1}$ | e |
| Praesepe‡ | 630 | $6.5 \times 10^{-2}$ | e | $3.5 \times 10^{-2}$ | e |

Previous studies have noted there may be a break off and steepening in the power law towards the highest flare energies (e.g. Chang et al. 2015). We note the possibility that this is the regime we have measured and that $\alpha$ at lower energies may be less than what we have measured. More observations of white-light flares from Orion-associated stars will allow us to further constrain $\alpha$ at the highest energies, by increasing the number of stars and rare high-energy flares observed.

### 3.2.1 *Comparison with other clusters*

Ilin et al. (2019) found from *K2* observations that between the 125 Myr Pleiades (M44) and 630 Myr Praesepe (M45) open clusters the average flare occurrence rate (for bolometric energies above $3.4 \times 10^{33}$ erg) of early M stars decreases quicker than the Skumanich $t^{-1/2}$ law. They found that the activity of hotter stars drops the quickest, tying in with previous observations of hotter stars spinning down more quickly than their cooler counterparts (e.g. Amard et al. 2019). The rate of this decrease, if it tracks with the change in surface rotation, is also expected to be variable at young ages (e.g. Barnes 2010). We can use our sample to try and extend this work for the highest energy flares down to stars of 4 Myr in age.

To measure the change in the flare rate for energies above $1 \times 10^{35}$ erg we have split our sample into the 3500–3750 and 3750–4000 K groups from Ilin et al. (2019). In each subset we have measured the rates directly by linearly interpolating the measured average occurrence rates to the value at $1 \times 10^{35}$ erg. To calculate the rates for the Pleiades and Praesepe we first multiplied the *Kepler* bandpass occurrence rates measured by Ilin et al. (2019) by 3.1 to convert them to bolometric energies, using the conversion factor from Paudel et al. (2018a). We then extrapolated these power laws to $1 \times 10^{35}$ erg.

For the 3500–3750 K sample the measured average occurrence rate of flares above $1 \times 10^{35}$ erg changes from 2.0 to $7.3 \times 10^{-2}$ and then to $6.5 \times 10^{-2}$ flares $yr^{-1}$ from Orion, through the Pleiades, to Praesepe. The change in this measured rate with age consequently goes from $-1.6 \times 10^{-2}$ to $-1.73 \times 10^{-5}$ flares $yr^{-1}$ $Myr^{-1}$. For the 3750–4000 K sample the rate of flares above $1 \times 10^{35}$ erg changes from 2.3 to $2.5 \times 10^{-1}$ and then to $3.5 \times 10^{-2}$. The change in this measured rate with age consequently goes from $-1.7 \times 10^{-2}$ to $-4.22 \times 10^{-4}$ flares $yr^{-1}$ $Myr^{-1}$. We can see that, from the change in the measured occurrence rate between open clusters, the observed activity of hotter stars (above $1 \times 10^{35}$ erg) is dropping at a faster rate in the first 600 Myr than cooler, lower mass, stars.

We also note that the change of occurrence rate of flares above $1 \times 10^{35}$ erg is not linear in log–log space, in disagreement with the model derived by Davenport et al. (2019). However, as noted in Section 3.2 flaring behaviour may change at the energies we are probing. These changes (e.g. breaks in power laws; Chang et al. 2015) were not included in the Davenport et al. (2019) model and as such a strict comparison may not be valid. We also note that the number of flares in our 3500–3750 and 3750–4000 K Orion subsets are five and six, respectively. The small sample size in these subsets combined with the extrapolation of the Ilin et al. (2019) occurrence rates means the values in Table 3 should be used with caution and best as estimates.

By combining these data sets together and linearly interpolating in age we can estimate the average flare rates for M stars in other clusters and associations. Some predictions for nearby young clusters are given in Table 3 for $E > 1 \times 10^{35}$ erg. We find that up to 70 Myr both samples can flare up to once a year with an energy above $1 \times 10^{35}$ erg.

### 3.2.2 *Formation of the radiative zone*

With an age of 4 Myr, the pre-main-sequence early M stars in Orion are fully convective. The magnetic fields of pre-main-sequence early M stars have previously been characterised as being large scale and axisymmetric. As these early M stars evolve they will contract and spin-up, something that seems counter-intuitive to a decrease in flare rates. However, during this process they begin to form an inner radiative zone that is separated from the outer convective regions by a tachocline. From the Baraffe et al. (2015) models this radiative zone reaches its maximum size at roughly 100 Myr. The formation of the radiative zone is expected to be accompanied by a change in the stellar magnetic topology and has previously been linked to observed decreases in the coronal X-ray luminosity (Gregory et al. 2016), which is often used as a tracer of magnetic activity (e.g. Wright et al. 2011). The transition between fully and partially convective interiors for main-sequence stars may also be linked to a decrease in the magnetic field strength, something previously noted by Mullan et al. (2018) (see fig. 14 of Moutou et al. 2017). It may be that the formation of a radiative zone for early M stars causes a drop in flare energies and rates between 4 and 125 Myr. After 125 Myr the average flare behaviour would more closely follow the decay of stellar rotation. Further observations of stars in Orion to confirm our measured average occurrence rates along with further observations of open clusters or moving groups with intermediate ages will be

needed to test this hypothesis for early M stars (e.g. the 30–40 Myr Octans group; Murphy & Lawson 2015) and other spectral types.

## 4 CONCLUSIONS

In this work, we have presented the detection of high-energy white-light stellar flares from 4.0 ± 0.2 Myr pre-main-sequence stars associated with the Orion Complex. These are some of the youngest stars to have a measured white-light flare occurrence rate. By combining our measured occurrence rates with those in the literature we identified that the rate of change in the average flare occurrence rate above $1 \times 10^{35}$ erg for M dwarfs is variable with time, appearing to change rapidly during the 100 Myr before slowing. This result is similar to findings for surface rotation. We have used these rates to predict the flare occurrence rates for nearby moving groups.

## ACKNOWLEDGEMENTS

We thank the referee for their help in greatly improving this paper. This research is based on data collected under the NGTS project at the ESO La Silla Paranal Observatory. The NGTS facility is funded by a consortium of institutes consisting of the University of Warwick, the University of Leicester, Queen's University Belfast, the University of Geneva, the Deutsches Zentrum für Luft- und Raumfahrt e.V. (DLR; under the 'Großinvestition GI-NGTS'), the University of Cambridge, together with the UK Science and Technology Facilities Council (STFC; project reference ST/M001962/1). JAGJ is supported by STFC PhD studentship 1763096. PJW is supported by STFC consolidated grant ST/P000495/1. EG gratefully acknowledges support from the David and Claudia Harding Foundation in the form of a Winton Exoplanet Fellowship.

This publication makes use of data products from the Two Micron All Sky Survey, which is a joint project of the University of Massachusetts and the Infrared Processing and Analysis Center/California Institute of Technology, funded by the National Aeronautics and Space Administration and the National Science Foundation. This publication makes use of data products from the *Wide-field Infrared Survey Explorer*, which is a joint project of the University of California, Los Angeles, and the Jet Propulsion Laboratory/California Institute of Technology, funded by the National Aeronautics and Space Administration. This work has made use of data from the European Space Agency (ESA) mission *Gaia* (https://www.cosmos.esa.int/gaia), processed by the *Gaia* Data Processing and Analysis Consortium (DPAC, https://www.cosmos.esa.int/web/gaia/dpac/consortium). Funding for the DPAC has been provided by national institutions, in particular the institutions participating in the *Gaia* Multilateral Agreement.

## DATA AVAILABILITY

Stellar and flare properties are available upon request to JAGJ.

## REFERENCES

Aguado D. S. et al., 2019, ApJS, 240, 23
Allard F., Homeier D., Freytag B., 2012, Philos. Trans. R. Soc. Lond. Ser. A, 370, 2765
Alstott J., Bullmore E., Plenz D., 2014, PLoS ONE, 9, e85777
Amard L., Palacios A., Charbonnel C., Gallet F., Georgy C., Lagarde N., Siess L., 2019, A&A, 631, A77
Ansdell M. et al., 2016, ApJ, 816, 69
Aschwanden M. J., Tarbell T. D., Nightingale R. W., Schrijver C. J., Title A., Kankelborg C. C., Martens P., Warren H. P., 2000, ApJ, 535, 1047
Bailer-Jones C. A. L., Rybizki J., Fouesneau M., Mantelet G., Andrae R., 2018, AJ, 156, 58
Baraffe I., Homeier D., Allard F., Chabrier G., 2015, A&A, 577, A42
Barnes S. A., 2010, ApJ, 722, 222
Bell C. P. M., Mamajek E. E., Naylor T., 2015, MNRAS, 454, 593
Benz A. O., Güdel M., 2010, ARA&A, 48, 241
Caramazza M., Flaccomio E., Micela G., Reale F., Wolk S. J., Feigelson E. D., 2007, A&A, 471, 645
Cardelli J. A., Clayton G. C., Mathis J. S., 1989, ApJ, 345, 245
Chang S. W., Byun Y. I., Hartman J. D., 2015, ApJ, 814, 35
Cody A. M. et al., 2014, AJ, 147, 82
Colombo S., Orlando S., Peres G., Reale F., Argiroffi C., Bonito R., Ibgui L., Stehlé C., 2019, A&A, 624, A50
Crosby N. B., Aschwanden M. J., Dennis B. R., 1993, Sol. Phys., 143, 275
Cutri R. M. et al., 2014, VizieR On-line Data Catalog: II/328
Davenport J. R. A., 2016, ApJ, 829, 23
Davenport J. R. A. et al., 2014, ApJ, 797, 122
Davenport J. R. A., Covey K. R., Clarke R. W., Boeck A. C., Cornet J., Hawley S. L., 2019, ApJ, 871, 241
Douglas S. T., Curtis J. L., Agüeros M. A., Cargile P. A., Brewer J. M., Meibom S., Jansen T., 2019, ApJ, 879, 100
Doyle J. G., Butler C. J., 1985, Nature, 313, 378
Epstein C. R., Pinsonneault M. H., 2014, ApJ, 780, 159
Favata F., Flaccomio E., Reale F., Micela G., Sciortino S., Shang H., Stassun K. G., Feigelson E. D., 2005, ApJS, 160, 469
Flaccomio E., Micela G., Sciortino S., Cody A. M., Guarcello M. G., Morales-Calderòn M., Rebull L., Stauffer J. R., 2018, A&A, 620, A55
Gaia Collaboration et al., 2016, A&A, 595, A2
Gaia Collaboration et al., 2018, A&A, 616, A1
Green G. M., Schlafly E., Zucker C., Speagle J. S., Finkbeiner D., 2019, ApJ, 887, 93
Gregory S. G., Adams F. C., Davies C. L., 2016, MNRAS, 457, 3836
Güdel M., Audard M., Kashyap V. L., Drake J. J., Guinan E. F., 2003, ApJ, 582, 423
Guo Z. et al., 2018, ApJ, 852, 56
Hawley S. L., Fisher G. H., 1992, ApJS, 78, 565
Hawley S. L., Davenport J. R. A., Kowalski A. F., Wisniewski J. P., Hebb L., Deitrick R., Hilton E. J., 2014, ApJ, 797, 121
Henden A., Munari U., 2014, Contr. Astron. Obser. Skalnate Pleso, 43, 518
Hilton E. J., Hawley S. L., Kowalski A. F., Holtzman J., 2011, in Johns-Krull C. M., Browning M. K., West A. A., eds, ASP Conf. Ser. Vol. 448, 16th Cambridge Workshop on Cool Stars, Stellar Systems, and the Sun. Astron. Soc. Pac., San Francisco, p. 197
Ilin E., Schmidt S. J., Davenport J. R. A., Strassmeier K. G., 2019, A&A, 622, A133
Jackman J. A. G. et al., 2018, MNRAS, 477, 4655
Jackman J. A. G. et al., 2019, MNRAS, 482, 5553
Jackson A. P., Davis T. A., Wheatley P. J., 2012, MNRAS, 422, 2024
Kounkel M. et al., 2018, AJ, 156, 84
Lacy C. H., Moffett T. J., Evans D. S., 1976, ApJS, 30, 85
Lin C. L., Ip W. H., Hou W. C., Huang L. C., Chang H. Y., 2019, ApJ, 873, 97
Matt S. P., Brun A. S., Baraffe I., Bouvier J., Chabrier G., 2015, ApJ, 799, L23
Moutou C. et al., 2017, MNRAS, 472, 4563
Mullan D. J., MacDonald J., Dieterich S., Fausey H., 2018, ApJ, 869, 149
Murphy S. J., Lawson W. A., 2015, MNRAS, 447, 1267
Orlando S., Reale F., Peres G., Mignone A., 2011, MNRAS, 415, 3380
Parker E. N., 1988, ApJ, 330, 474
Paudel R. R., Gizis J. E., Mullan D. J., Schmidt S. J., Burgasser A. J., Williams P. K. G., Berger E., 2018a, ApJ, 858, 55
Paudel R. R., Gizis J. E., Mullan D. J., Schmidt S. J., Burgasser A. J., Williams P. K. G., Berger E., 2018b, ApJ, 861, 76
Pecaut M. J., Mamajek E. E., 2013, ApJS, 208, 9
Pravdo S. H., Angelini L., 1995, ApJ, 447, 342
Shibayama T. et al., 2013, ApJS, 209, 5

Shimizu T., 1995, PASJ, 47, 251
Skrutskie M. F. et al., 2006, AJ, 131, 1163
Skumanich A., 1972, ApJ, 171, 565
Stelzer B., Flaccomio E., Briggs K., Micela G., Scelsi L., Audard M., Pillitteri I., Güdel M., 2007, A&A, 468, 463
Strom K. M. et al., 1990, ApJ, 362, 168
Wheatley P. J. et al., 2018, MNRAS, 475, 4476
Wright N. J., Drake J. J., Mamajek E. E., Henry G. W., 2011, ApJ, 743, 48
Yang H., Liu J., 2019, ApJS, 241, 29

## APPENDIX A: THE SMALLEST AND LARGEST DETECTED FLARES

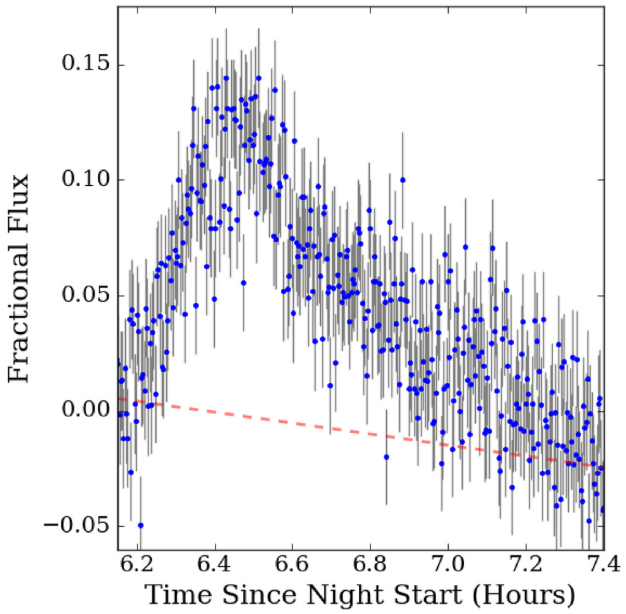


**Figure A1.** The lowest amplitude flare detected in our sample. The red dashed line is an example of the baseline used when calculating flare energies, as discussed in Section 2.3.

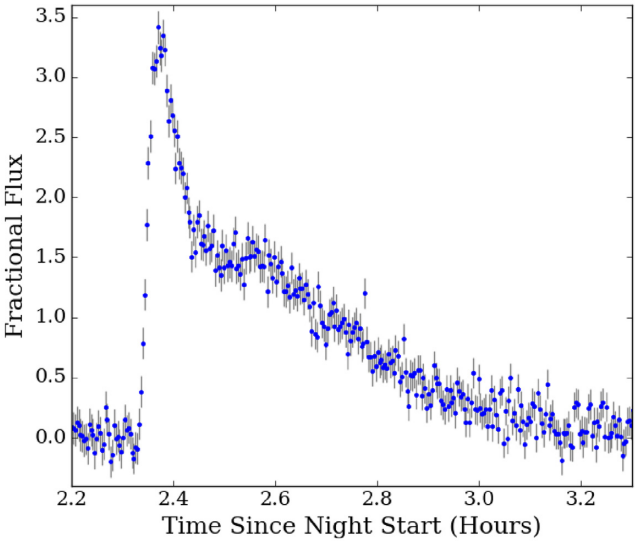


**Figure A2.** The highest amplitude flare detected in our sample.

## APPENDIX B: EARLY M STARS AND THEIR COMPLETENESS ENERGIES

**Table B1.** Detected flares, their energies, and the 68 per cent completeness energies for the stars in the full 3400–3940 K sample. The final column indicates whether this star was used in our calculation of the flare occurrence rate in Section 3.2.

| 2MASS source ID | *Gaia* DR2 source ID | SpT | SpT source | Flare energy (erg) | Completeness energy (erg) | Used? |
|---|---|---|---|---|---|---|
| 2MASS J05265619−0706548 | 3016662403101758720 | M0.5 | SED | $9.64^{+3.44}_{-2.53} \times 10^{34}$ | $7.26 \times 10^{34}$ | Y |
| 2MASS J05265619−0706548 | 3016662403101758720 | M0.5 | SED | $1.01^{+0.32}_{-0.24} \times 10^{35}$ | $7.26 \times 10^{34}$ | Y |
| 2MASS J05312392−0709304 | 3016615055382512768 | M0 | SED | $4.24^{+0.94}_{-0.77} \times 10^{34}$ | $6.42 \times 10^{34}$ | Y |
| 2MASS J05313541−0710550 | 3016614402547478784 | M1.5 | SED | $1.76^{+0.38}_{-0.31} \times 10^{35}$ | $5.52 \times 10^{34}$ | Y |
| 2MASS J05314319−0717409 | 3016424736790884736 | M1.5 | SED | $1.40^{+1.33}_{-0.68} \times 10^{35}$ | $4.38 \times 10^{34}$ | Y |
| 2MASS J05340216−0717390 | 3016505963212457088 | M3 | SED | $2.70^{+1.02}_{-0.74} \times 10^{34}$ | $6.51 \times 10^{34}$ | Y |
| 2MASS J05340216−0717390 | 3016505963212457088 | M3 | SED | $6.98^{+2.51}_{-1.85} \times 10^{34}$ | $6.51 \times 10^{34}$ | Y |
| 2MASS J05340216−0717390 | 3016505963212457088 | M3 | SED | $3.68^{+1.40}_{-1.01} \times 10^{35}$ | $6.51 \times 10^{34}$ | Y |
| 2MASS J05350988−0718045 | 3016457000585375872 | M2 | SED | $1.70^{+0.40}_{-0.32} \times 10^{35}$ | $6.79 \times 10^{34}$ | Y |
| 2MASS J05351113−0719063 | 3016456210311395456 | M1 | SED | $9.08^{+2.66}_{-2.06} \times 10^{34}$ | $7.83 \times 10^{34}$ | Y |
| 2MASS J05273635−0744059 | 3015081163645266304 | M1.5 | SED | $5.64^{+1.64}_{-1.27} \times 10^{34}$ | $6.09 \times 10^{34}$ | Y |
| 2MASS J05350942−0749194 | 3015674698061271936 | M3 | SED | $3.09^{+0.88}_{-0.68} \times 10^{35}$ | $1.58 \times 10^{35}$ | N |
| 2MASS J05293055−0754194 | 3014873669481488896 | M1.5 | SED | $2.54^{+0.42}_{-0.36} \times 10^{34}$ | $6.64 \times 10^{34}$ | Y |
| 2MASS J05340890−0912415 | 3013742546894832384 | M0.5 | SED | $6.66^{+1.91}_{-1.49} \times 10^{33}$ | $6.03 \times 10^{34}$ | Y |
| 2MASS J05340890−0912415 | 3013742546894832384 | M0.5 | SED | $1.08^{+0.31}_{-0.24} \times 10^{35}$ | $6.03 \times 10^{34}$ | Y |

**Table B2.** 68 per cent completeness energies for all the stars in our 3400–3940 K samples. This includes both the flaring the non-flaring stars. The final column indicates whether this star was used in our calculation of the flare occurrence rate in Section 3.2. K18 indicates the spectral type is taken from Kounkel et al. (2018).

| 2MASS source ID | *Gaia* DR2 source ID | SpT | SpT source | Completeness energy (erg) | Used? |
|---|---|---|---|---|---|
| 2MASS J05265619−0706548 | 3016662403101758720 | M0.5 | SED | $7.26 \times 10^{34}$ | Y |
| 2MASS J05344294−0703497 | 3016533996462888192 | M0.5 | SED | $7.26 \times 10^{34}$ | Y |
| 2MASS J05302813−0706421 | 3016629417753191424 | M1.5 | SED | $3.64 \times 10^{34}$ | Y |
| 2MASS J05362055−0705317 | 3016488955142025984 | M0 | K18 | $1.11 \times 10^{35}$ | N |
| 2MASS J05313128−0708564 | 3016615261540932224 | M3 | SED | $1.35 \times 10^{35}$ | N |
| 2MASS J05312392−0709304 | 3016615055382512768 | M0 | SED | $6.42 \times 10^{34}$ | Y |
| 2MASS J05313541−0710550 | 3016614402547478784 | M1.5 | SED | $5.52 \times 10^{34}$ | Y |
| 2MASS J05335093−0711038 | 3016510911014768512 | M1.5 | SED | $6.52 \times 10^{34}$ | Y |
| 2MASS J05343263−0715180 | 3016460883235690624 | M3 | SED | $7.47 \times 10^{34}$ | Y |
| 2MASS J05314319−0717409 | 3016424736790884736 | M1.5 | SED | $4.38 \times 10^{34}$ | Y |
| 2MASS J05290015−0719465 | 3016598837585920512 | M1 | SED | $5.99 \times 10^{34}$ | Y |
| 2MASS J05340216−0717390 | 3016505963212457088 | M3 | SED | $6.51 \times 10^{34}$ | Y |
| 2MASS J05350988−0718045 | 3016457000585375872 | M2 | SED | $6.79 \times 10^{34}$ | Y |
| 2MASS J05313990−0719450 | 3016423053163711488 | M2 | SED | $7.34 \times 10^{34}$ | Y |
| 2MASS J05325564−0720064 | 3016501874403636480 | M3 | SED | $1.46 \times 10^{35}$ | N |
| 2MASS J05351113−0719063 | 3016456210311395456 | M1 | SED | $7.83 \times 10^{34}$ | Y |
| 2MASS J05351686−0719019 | 3016455969793224192 | M1 | SED | $8.38 \times 10^{34}$ | Y |
| 2MASS J05351770−0720152 | 3016455866714010880 | M1 | SED | $9.94 \times 10^{34}$ | N |
| 2MASS J05305836−0722365 | 3016417212008224896 | M2 | SED | $4.66 \times 10^{34}$ | Y |
| 2MASS J05291038−0724262 | 3016594576978615936 | M3 | SED | $6.76 \times 10^{34}$ | Y |
| 2MASS J05322860−0724037 | 3016408141037780736 | M3 | SED | $4.54 \times 10^{34}$ | Y |
| 2MASS J05341974−0720320 | 3016457893938475904 | M2 | SED | $7.38 \times 10^{34}$ | Y |
| 2MASS J05344904−0726070 | 3016453152294702848 | M2 | SED | $5.70 \times 10^{34}$ | Y |
| 2MASS J05332977−0726348 | 3016450571017334016 | M1.5 | K18 | $3.68 \times 10^{35}$ | N |
| 2MASS J05355628−0728317 | 3016438549405961472 | M1.5 | SED | $5.14 \times 10^{34}$ | Y |
| 2MASS J05295064−0734543 | 3016576366317290240 | M1 | SED | $5.39 \times 10^{34}$ | Y |
| 2MASS J05273635−0744059 | 3015081163645266304 | M1.5 | SED | $6.09 \times 10^{34}$ | Y |
| 2MASS J05320092−0745170 | 3016344644241021824 | M2.5 | SED | $1.24 \times 10^{35}$ | N |
| 2MASS J05293238−0747456 | 3016378832180580352 | M2 | SED | $1.50 \times 10^{35}$ | N |
| 2MASS J05350942−0749194 | 3015674698061271936 | M3 | SED | $1.58 \times 10^{35}$ | N |
| 2MASS J05293055−0754194 | 3014873669481488896 | M1.5 | SED | $6.64 \times 10^{34}$ | Y |
| 2MASS J05343717−0757402 | 3015575398418115456 | M0.5 | K18 | $1.08 \times 10^{35}$ | N |
| 2MASS J05361957−0759448 | 3015653532462547200 | M2 | SED | $1.89 \times 10^{35}$ | N |
| 2MASS J05304518−0804494 | 3016309116271690240 | M2 | SED | $4.89 \times 10^{34}$ | Y |
| 2MASS J05313203−0809001 | 3016305645938094592 | M2.5 | SED | $5.67 \times 10^{34}$ | Y |
| 2MASS J05344653−0818539 | 3015547807548427264 | M2.5 | SED | $1.60 \times 10^{35}$ | N |
| 2MASS J05281520−0844070 | 3014757258688194048 | M2 | SED | $7.26 \times 10^{34}$ | Y |
| 2MASS J05371561−0859214 | 3015242177675724032 | M0 | SED | $7.34 \times 10^{34}$ | Y |
| 2MASS J05340890−0912415 | 3013742546894832384 | M0.5 | SED | $6.03 \times 10^{34}$ | Y |

This paper has been typeset from a TEX/LATEX file prepared by the author.